AFRL-RY-WP-TR-2020-0074

A NEW CONCEPTUAL MODEL FOR LAMINAR BOUNDARY LAYER FLOW

David Weyburne
EO/IR Components Branch
Aerospace Components & Subsystems Division

APRIL 2020
Final Report

AIR FORCE RESEARCH LABORATORY
SENSORS DIRECTORATE
WRIGHT-PATTERSON AIR FORCE BASE, OH 45433-7320
AIR FORCE MATERIEL COMMAND
UNITED STATES AIR FORCE

REPORT DOCUMENTATION PAGE

Form Approved
OMB No. 0704-0188

1. REPORT DATE *(DD-MM-YY)*	2. REPORT TYPE	3. DATES COVERED *(From - To)*
April 2020	Final	1 December 2014 –13 April 2015

4. TITLE AND SUBTITLE
A NEW CONCEPTUAL MODEL FOR LAMINAR BOUNDARY LAYER FLOW

5a. CONTRACT NUMBER
In-House

5b. GRANT NUMBER

5c. PROGRAM ELEMENT NUMBER
61102F

6. AUTHOR(S)
David Weyburne

5d. PROJECT NUMBER
3001

5e. TASK NUMBER
N/A

5f. WORK UNIT NUMBER
Y02E

7. PERFORMING ORGANIZATION NAME(S) AND ADDRESS(ES)

EO/IR Components Branch, Aerospace Components & Subsystems Division
Air Force Research Laboratory, Sensors Directorate (AFRL/RYDH)
Wright-Patterson Air Force Base, OH 45433-7320
Air Force Materiel Command, United States Air Force

8. PERFORMING ORGANIZATION REPORT NUMBER

9. SPONSORING/MONITORING AGENCY NAME(S) AND ADDRESS(ES)

Air Force Research Laboratory
Sensors Directorate
Wright-Patterson Air Force Base, OH 45433-7320
Air Force Materiel Command
United States Air Force

Air Force Office of Scientific Research Public Affairs (AFOSR)
875 North Randolph Street, Suite 325, Room 3112
Arlington, VA 22203

10. SPONSORING/MONITORING AGENCY ACRONYM(S)
AFRL/RYDH

11. SPONSORING/MONITORING AGENCY REPORT NUMBER(S)
AFRL-RY-WP-TR-2020-0074

12. DISTRIBUTION/AVAILABILITY STATEMENT
Approved for public release; distribution is unlimited.

13. SUPPLEMENTARY NOTES
PAO case number 88ABW-2019-6049, Clearance Date 20 December 2019. This work was funded in whole or in part by Department of the Air Force. Report contains color.

14. ABSTRACT

Computer simulation results indicate that the traditional Blasius laminar flow treatment does not describe the boundary layer flow correctly. The problem is found to be the traditional conceptual model for the boundary layer, it is flawed. The fix is to apply the unbounded and bounded boundary layer concepts introduced in an earlier report. Herein we flesh out the unbounded boundary layer concept applied to laminar flow along a wall. The Blasius model is found to represent the viscous region and approximate analytical solutions are found for the inertial region. The new model is comparable to simulation. The new conceptual models have implications for turbulent flows and wind tunnel experiments.

15. SUBJECT TERMS
boundary layer theory, unbounded boundary layer, blasius model, inertial boundary layer, laminar flow, flat plate

16. SECURITY CLASSIFICATION OF:			17. LIMITATION OF ABSTRACT:	18. NUMBER OF PAGES	19a. NAME OF RESPONSIBLE PERSON (Monitor)
a. REPORT	b. ABSTRACT	c. THIS PAGE			David Tomich
Unclassified	Unclassified	Unclassified	SAR	34	19b. TELEPHONE NUMBER *(Include Area Code)* N/A

Table of Contents

Section **Page**

List of Figures

Figure **Page**

1. SUMMARY

The boundary layer flow concept originally developed by Ludwig Prandtl is often depicted in terms of fluid flowing over a flat plate. The Blasius theoretical model describes the laminar flow case for this flow situation and this association to the depiction of the boundary layer concept has earned it a prominent position in boundary layer literature. The fact that wind tunnel experiments can routinely generate Blasius velocity profiles by inducing a zero-pressure gradient in the flow direction (part of the Blasius model) has only reinforced the prominence of the Blasius model. This success comes in spite of a number of serious theoretical problems that have been identified with the model. Recently, it was pointed out (AF Tech Report AFRL-RY-WP-TR-2019-0002) that based on simulation results, the apparent agreement between the Blasius model and experimental wind tunnel results is not as good as previously believed. While the velocity profiles for the flow direction velocity look correct, the normal velocity profiles and the normal pressure gradient profiles do not. It was concluded that the Blasius theoretical model does not correctly describe the flow situation typically encountered in wind tunnel experiments. This failure led us to reevaluate the Blasius model and the traditional boundary layer concept. After close examination, we find that the traditional interpretation of the boundary layer concept is flawed. It incorrectly mixes aspects of both interior flows and exterior flows. These problems are corrected with the bounded and unbounded boundary layer concepts introduced in the earlier mentioned AF Tech Report. Herein, we show the adoption of the new unbounded boundary layer model also corrects most of the problems with Blasius model. The key feature of this unbounded boundary layer flow is that the velocity peaks near the boundary layer edge and slowly decreases to the free stream velocity. This is the type of boundary layer encountered in exterior flows such as those on airplane wings in free flight. It is also the type of boundary layer encountered when the wind tunnel height becomes very large (according to the simulation results). This new boundary layer concept provides the basis for a new theoretical model to describe laminar flow along a flat plate. The unbounded boundary layer is first divided into two regions; the near wall viscous region and the inertial boundary layer region. The Blasius theoretical model is found to describe the near wall region. To develop a theoretical model of the inertial region, we first examine computer simulations to try to understand the velocity and pressure behavior in the inertial boundary layer region. For a 2-D channel flow, the channel gap must be at least 200-meters for the flow to reach the unbounded boundary layer flow behavior. A simple exponential velocity approximation is found to work for the inertial velocity profile for this flow situation. The resulting complete theoretical model is found to give reasonable approximations to the simulation result for laminar flow on a flat plate. The new results are used to flesh out the new bounded and unbounded boundary layer concepts is in terms of the physics that is driving the fluid flow in the boundary layer region. We also discuss the implications for turbulent flows and for interpreting wind tunnel experiments.

2. INTRODUCTION

Ludwig Prandtl's[1] boundary layer concept for steady laminar flow along a wall is often depicted as shown in Fig. 1. The no-slip boundary condition results in a zero velocity at the wall. The velocity $u(x, y)$ monotonically increases above the plate until it asymptotes to the velocity at the boundary layer edge, $u_e(x)$. The boundary layer thickness slowly increases as we move along the wall due to a buildup of slow-moving fluid. Blasius,[2] one of Prandtl's students, developed the theoretical model corresponding to the flow for the case where the boundary layer edge velocity is just the free stream velocity u_0 corresponding to the zero-pressure gradient (ZPG) condition. The close association with the conceptual model for boundary layer flow has insured a prominent place for the Blasius theoretical model. The Blasius model appears in almost every fluid flow textbook as an introduction to boundary layer flow and as well as an introduction to similarity theoretical solutions to boundary layer flows. The universal acceptance of this model appears to be partly driven by the association between the conceptual depiction and the theoretical model, partly by the simplicity of the model, and partly by the fact that wind tunnel measurements seem to confirm its existence. Nikuradse's[3] experimental wind tunnel results featured in Schlichting's[4] seminal book on boundary layer theory is a powerful confirmation of the Blasius theory in particular and the boundary layer concept in general. The universal acceptance of the model, fueled by the wind tunnel experiments, has resulted in the Blasius theoretical model being routinely used as a way to verify proper wind tunnel configuration/operation[5,6] as well as a way to verify computer flow simulation computational engines.[7,8]

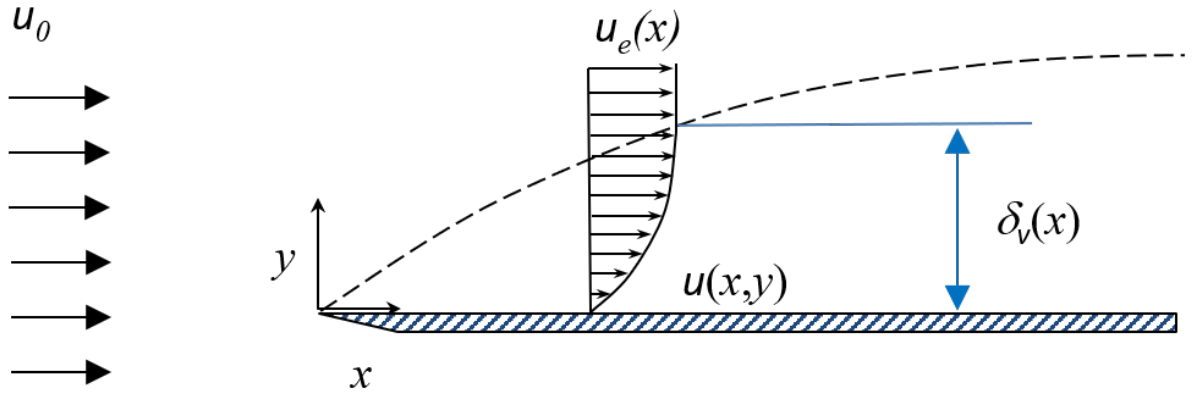

Figure 1: Traditional depiction of the 2-D boundary layer along a sei-infinite flat plate.

However, a closer look at the Blasius model reveals a number of disturbing discrepancies that one would not expect for fluid flow along a flat plate. The most serious problem with the Blasius solution is that the calculated normal to the wall velocity[9-11] and the normal to the wall pressure gradient[12] are both finite at an infinite distance from the wall. This is obviously non-physical. There have been a number of not very satisfying attempts to explain this away (see, for example, Lewins[9] and Panton[10]). More recently, Weyburne[13] pointed out another problem with

the Blasius model. In the Blasius model, the pressure gradient in the flow direction is assumed to be zero in the boundary layer region. This assumption cannot be correct. There can be no flow without a driving force but just as problematic is that the pressure forces in the boundary layer that induce the normal velocity flow must also affect the pressure gradient in the flow direction since pressure affects cannot be unidirectional. The consequences of this non-zero pressure gradient in the flow direction is that there should be a velocity overshoot at the boundary layer edge. This behavior is not observed in the Blasius model. In spite of all of these problems, it is widely believed that the Blasius model is mostly correct but with these unresolved issues that have been largely ignored.

The reason for this near universal acceptance of the theory in spite of these problems is that the wind tunnel and CFD experimental results seem to confirm the Blasius model. However, this apparent experimental confirmation needs to be re-evaluated. Recently we set up a series of computer simulation experiments[13] that, in part, tried to verify the existence of Blasius type flow in a 2D channel with typical wind tunnel dimensions (1-meter high by 8-meter long). It was found that zero-degree incident flow did not produce Blasius type flow for 2D channel airflow at room temperature. This result appears to correspond to actual wind tunnel experiments and is not unexpected since the pressure gradient in the flow direction will not be zero under these conditions. One standard wind tunnel technique (see, for example, Jovanović, *et. al.*[5]) to induce a zero-pressure gradient along the tunnel plate and thereby generate Blasius profiles is to slightly tilt one of the tunnel plates. And, in fact, the simulation results[13] for the small angle tilted wall case showed that it is possible to produce $u(x, y)$ velocity profiles that behaved similarly when scaled with the Blasius scaling parameters. However, the normal velocity $v(x, y)$ profiles and the dP/dy pressure gradient profiles did not show similarity for Blasius scaling's under these same conditions. Overall, it was concluded that the small angle wedge flow is not well represented by the Blasius theoretical model. To induce an even flatter near-zero pressure gradient, attempts were also made using a curved/tilted top plate. This technique is also routinely used in wind tunnels (see, for example Harun, *et. al.*[14]) to force the flow to take on a variety of pressure gradient conditions including the ZPG case. While effective in forcing a near-zero pressure gradient and Blasius-like $u(x, y)$ velocity profiles, the Blasius scaling parameters did not show similar behavior for the normal velocity profiles or the normal pressure gradient profiles no matter what was tried on the one meter gapped channel.[13] Although the simulation result needs to be verified, as it stands, the assumption that the Blasius theoretical model describes steady 2-D laminar flow along a tilted or not tilted flat plate in a wind tunnel is not correct.

How can this be possible? Many experiments (see, for example, Ref. 3, 5, 6, and 15) have demonstrated Blasius profiles in wind tunnels yet the simulation results appear to contradict these results. In all the wind tunnel experiments, it is only the $u(x, y)$ velocity profiles that are measured and shown to agree with the Blasius profile. The normal velocity $v(x, y)$ for the flat plate case is on the order of 1/1000 of the $u(x, y)$ velocity making it difficult to measure $v(x, y)$ profiles in a wind tunnel situation. For that reason, the normal velocity profile is rarely measured. The same is true of the pressure gradient dP/dy profiles. Hence, the assumption that the wind tunnel results confirm to the Blasius theoretical model has never been fully tested.

If the simulation results are valid, and we have no reason to believe they are not, then this would mean that the Blasius theoretical model no longer enjoys the wind tunnel experimental verification support that it has had in the past. This, in turn, brings the theoretical problems already mentioned into a stronger light. And it should be problematic that the boundary layer theory that is so closely associated with the traditional boundary layer concept predicts such unrealistic physical manifestations far from the wall.

However, there is a way forward. Herein, we reapply the Blasius theoretical model in a context that removes the theoretical problems. The key is not the theoretical model but the conceptual model for the boundary layer. In an earlier set of AF Tech Reports,[13,16] we introduced what we termed the "unbounded" and "bounded" boundary layer concepts corresponding to boundary layers formed in exterior and interior flow situations. The unbounded boundary layer concept is depicted in Fig. 2. For the unbounded boundary layer case, the velocity profile goes through a maximum near the viscous boundary layer edge and then slowly declines to the free stream velocity. This is the type of boundary layer encountered for exterior flow like that for airflow over a wing[16] in flight. On the other hand, for flow in a typical wind tunnel, the presence of the ceiling produces pressure fields that interact with the plate boundary layer. This ends up producing asymptotic boundary layer flows that look like those depicted in Fig. 1. This interacting boundary layer condition is what we have termed the "bounded" boundary layer and is by definition an interior flow situation. The traditional interpretation of Fig. 1 is that there is no upper bound unlike that of an interior flow. This flawed mixed flow interpretation is one of the reasons for the Blasius theoretical problems. We discuss the problem more fully in the Discussion section below.

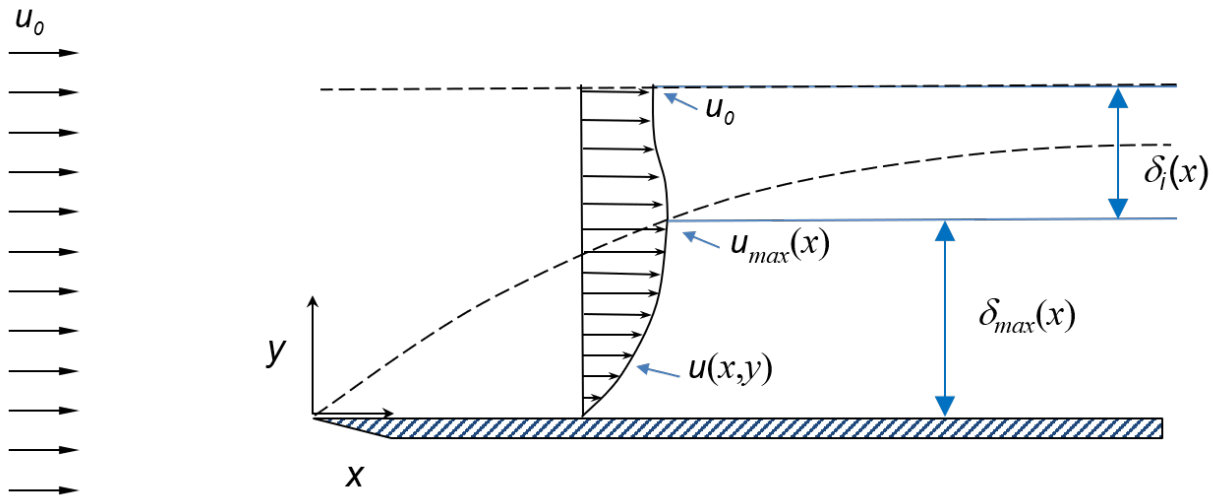

gure 2: Schematic depicting an unbounded 2-D laminar boundary layer along a semi-infinite flat plate.

The tie-in between the new "unbounded" boundary layer concept and the Blasius theoretical model was discovered during the earlier mentioned simulation study.[13] The simulations used a large gap 2D flat plate channel geometry where the gap varied from 1-meter typical in many wind tunnels to a gap of 20-meters meant to simulate the unbounded flow state. It was found that once the channel gap exceeded about 10-meters, the near wall flow started to behave like the

Blasius theoretical model, including the normal velocity and normal pressure gradient. Note that this ZPG-like condition occurs without having to tilt the channel plates. These results are similar to those of Vaughn who did a simulation study to try to determine the proper simulation outer limit extents for external flows.[17]

The association between the unbounded boundary layer and the Blasius theoretical model has a distinct advantage. For theoretical convenience, we can divide the unbounded boundary layer into two regions: the first is the viscous region which closely mimics the traditional viscous boundary layer, and the second region we termed the inertial region since viscous forces are mostly absent. This is the key to applying the Blasius theoretical model. Now we have a physical and logical justification for applying the viscous Blasius model to the just the near wall region. In the inertial region of the boundary layer, the velocity slowly returns to the free stream velocity. The transition between the two regions depends on how one defines the viscous effects range. Using the viscous thickness defined by the moment method, we showed that this transition occurs close to the $u_{max}(x)$, the velocity overshoot maximum at $\delta_{\max}$.[13,16] In our new theoretical approach, we assume that a suitably modified Blasius model applies to the region between the wall and $\delta_{\max}$. For the inertial boundary layer region, we introduce approximate solutions using the Blasius asymptotic solution at $\delta_{\max}$ as the lower boundary condition. In order to develop the approximate solutions to the inertial region, it is necessary to understand the pressure and velocity fields in this region. We have very little information on this region at the present time.[13,16] To remedy this, in what follows, we undertake an extended simulation study of the unbounded boundary layer situation for laminar flow. We use the results to develop and justify approximate velocity and pressure gradients in the inertial region. The resulting new theoretical model for unbounded laminar flow on a flat plate is then compared to the simulation results.

Finally, in the Discussion section, the new results are used to flesh out the unbounded and bounded boundary layer concepts in terms of interior and exterior flows and the physics that is driving the fluid flow in the boundary layer region. The problems with the traditional boundary layer concept are discussed and how the bounded and bounded boundary layer concepts correct the deficiencies. The implications of the new model for turbulent flows and for interpreting wind tunnel experiments is also discussed.

3. SIMULATION OF A LARGE GAP 2-D CHANNEL

The objective of the effort herein is to develop a new theoretical model for laminar flow over a flat plate and gain insight into the physics underlying the unbounded boundary layer concept. This requires an understanding of the behavior of the velocity and pressure gradients induced by the plate on the flow in the inertial part of the boundary layer. Since little is known about this behavior, we undertake a simulation effort. Rather than modeling a free-standing plate, we choose to model a 2-D large gap channel since this geometry can mimic the flat plate flow depicted in Fig. 2 for the case where the channel gap becomes very large. To avoid wake effects, we set the flow exit at the channel exit. The main difference between the simulation herein and the earlier effort[13] is that we extend the inlet section (no walls) to 20-meters as opposed to 0.5-meters used in the earlier effort. The earlier effort was an attempt to mimic an actual wind tunnel whereas herein we are interested in trying to accurately resolve the effects of the channel inlet edges on the velocities and pressure gradients. A side view of the initial simulation geometry is depicted in Fig. 3. The channel gap was varied from 10-meters to 200-meters. The exit Reynolds number is set to $Re_x = 5x10^5$ by setting the inlet velocity to 0.9375 *m/s* of room temperature (RT) airflow thereby eliminating turbulent concerns. OpenFoam simulation software is used with multi-grade meshing in both the flow direction and normal to the wall

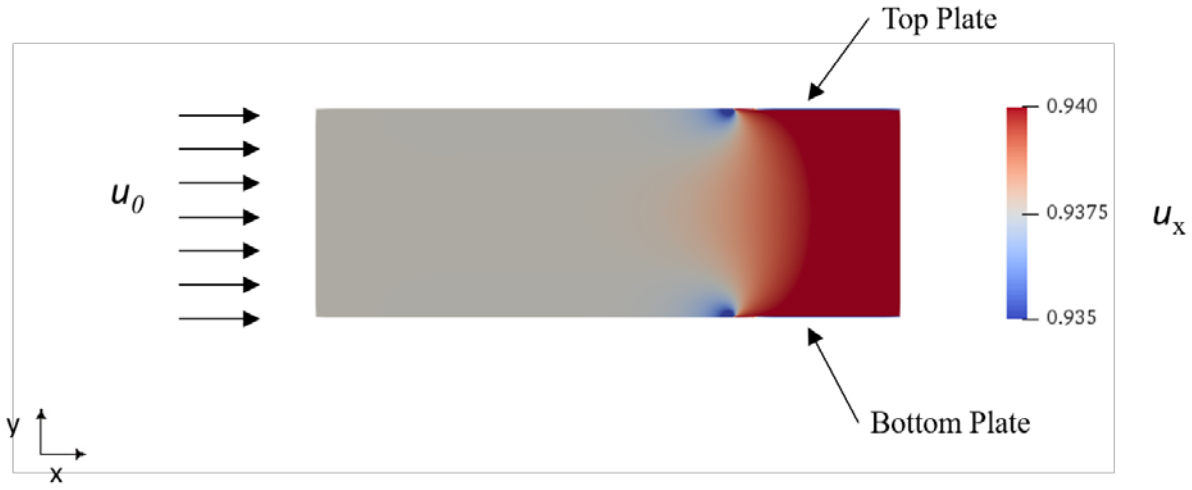

Figure 3: Side view of simulated air flow in a 10-meter high by 8-meter long channel with a 20-meter inlet section. The inlet velocity u_0 is 0.9375 *m/s* air flow at RT.

directions. The SimpleFoam solver is used, incompressibility imposed, and the exit set to a zero-pressure boundary condition. Mesh sizes are 2000 by 1000. The simulations are run until the velocity and pressure residuals dropped below $1x10^{-6}$. Verification is accomplished with a four-block mesh, single plate simulation with the upper boundary set to zero gradient condition. The 100-*m* high simulated results are almost identical to the 200-*m* channel result.

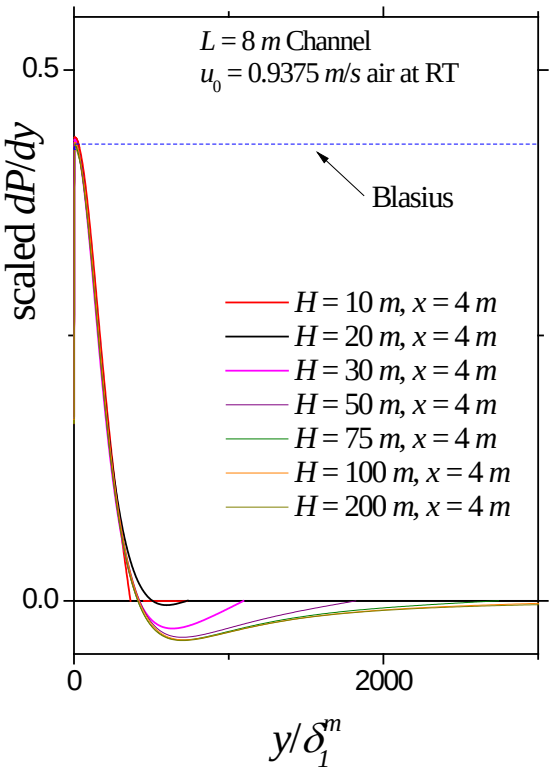

Figure 4: The half channel *y*-pressure gradient for various channel gaps.

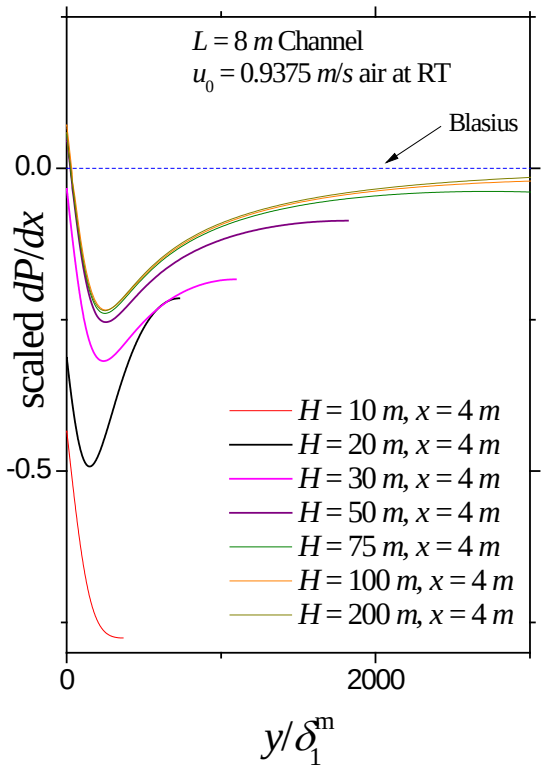

Figure 5: The half channel *x*-pressure gradient for various channel gaps.

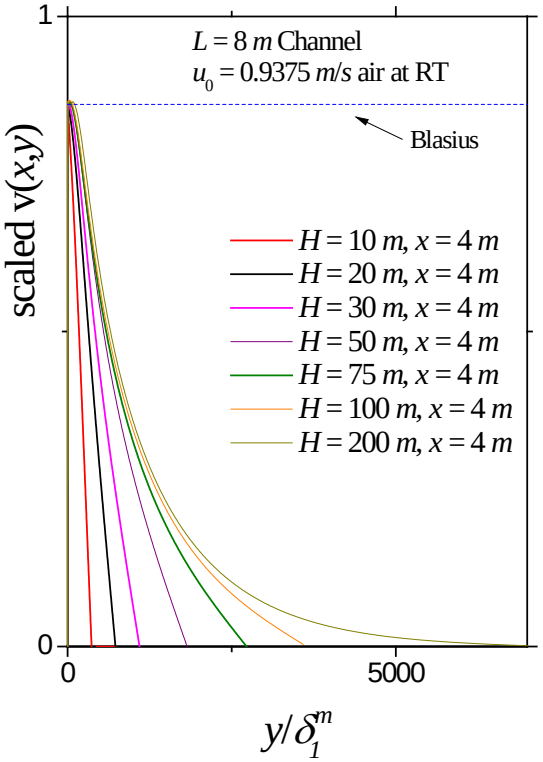

Figure 6: The half channel *v*(*x*,*y*) profiles for various channel gaps.

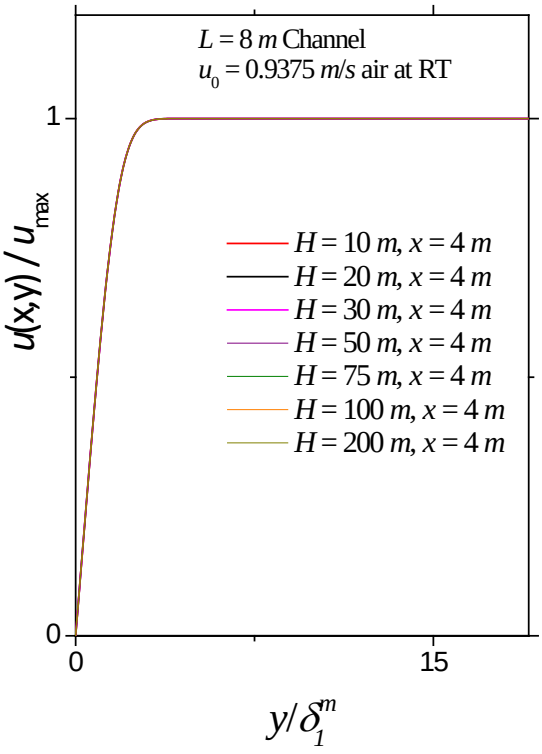

Figure 7: The half channel *u*(*x*,*y*) profiles for various channel gaps.

In Figs. 4-7 we plot the two scaled half channel pressure gradients profiles and the two scaled velocity profiles at a fixed position along the channel (x/L = 4) for different channel gaps. The first observation to be made is that all of these profiles would look very different in a real wind tunnel. In fact, all of these profiles would look essentially constant since the pressure and velocity measurement dynamic range is too limited to resolve these features at the present time. We will come back to this point in the Discussion section.

The pressure gradients in Figs. 4 and 5 are scaled using the similarity scaling parameters appropriate to the near wall region. The *y*-values are scaled by the maximum displacement thickness $\delta_1^m(x)$ which is the traditional displacement thickness but with $u_{\max}$ replacing u_0 (Appendix A). The pressure gradients are scaled by $u_{\max}^{3/2}\sqrt{\nu}/x^{3/2}$ where ν is the kinematic viscosity.[12]

The scaled *y*-pressure gradient profile plots (Fig. 4) peak at $y = \delta_{\max}$ and then decrease almost linearly to zero but with some undershoot. As the gap is increased, the *y*-pressure gradient appears to asymptote to a curve something close to the *H*=200 *m* case. The *H*=100 *m* and *H*= 200 *m* cases plot on top of one another and slowly asymptote to zero. We believe these curves represent the unbounded boundary layer case. Also included in this figure is the Blasius result[12] (asymptote value is 0.4302) to emphasize the unphysical nature for the traditional

boundary layer concept. The *x*-pressure gradients in Fig. 5 also show the slow asymptote to zero behavior for the largest gaps. The *H*=100 *m* and *H*=200 *m* cases, as with the d*P*/d*y* case, plot on top of one another further reinforcing our assumption that these represent unbounded boundary layer cases.

The normal $v(x, y)$ velocity profiles as a function of the channel gap are plotted in Fig. 6. The normal velocity profiles in Fig. 6 (and all $v(x, y)$ profiles herein) are scaled by $\sqrt{\nu u_{\max}/x}$. Notice that only the *H*=200 *m* gap shows a slow asymptotic decay to zero. This means that the inertial boundary layer thickness is somewhere between *H*=100 *m* and *H*=200 *m* for the conditions used herein. Also included in this figure is the Blasius result (asymptote value is 0.8604) to emphasize the unphysical nature for the traditional boundary layer concept.

We found that in contrast to the other profiles, the $u(x, y)$ velocity profiles show almost no change with the channel gap. All the profiles plot on top of one another. They also plot on top of the Blasius theoretical solution. We scaled the profiles with u_{max} but u_{max} only varied by less than 0.1% for the channel gaps between *H*=10 *m* and *H*=200 *m* indicating the profiles are nearly identical.

The results of Figs. 4-7 indicate that the expected asymptotic approach to zero behavior occurs when the channel gap reaches 100 *m* to 200 *m*. This means that the "unbounded" boundary layer thickness is somewhere in this range for these conditions. This result is reinforced by comparing the calculated two-sigma inertial boundary layer thickness described previously[16] to the half channel value shown in Fig. 8. At the lower channel gaps, the calculated δ_i value is pinned to

the half channel thickness but becomes unpinned starting around 75 *m*. For reference, this half channel thickness corresponds to 882 times the viscous boundary layer thicknesses.

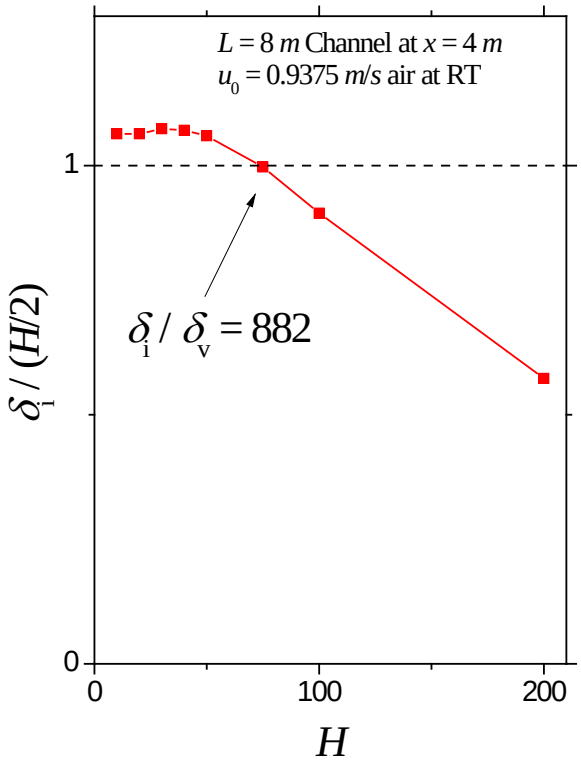

Figure 8: The inertial boundary layer thickness compared to the channel half height for various channel gaps.

Figs. 4-7 examined the pressure gradients and velocity profiles as a function of the channel gap. The results, along with Fig. 8, indicate that the "unbounded" flow case is not reached until the channel gap somewhere between *H*=100 *m* and *H*=200 *m* for these flow conditions. Therefore, we choose the *H*=200 *m* case as representative of the unbounded laminar flow case for flow along a flat plate. In Figs. 9-13 we plot the pressures, pressure gradients, and velocities profiles at various locations along the channel plate for the *H*=200 *m* case. The set of figures (Figs. 9-13) are close to what we believe the unbounded boundary layer profiles should look like.

The pressure plots in Fig. 9 give an important insight into the behavior that is driving the flow in the inertial part of the boundary layer. In Fig. 9a we see that the largest pressure variations are at locations at the front of the plate. This means that the pressure disturbance at the channel plate inlet edge is a major contributor to the pressure behavior in the inertial boundary layer region. The pressure peaks are relatively small at about 0.1% of atmospheric pressure. The maximum pressure peak at each location occurs at about $270\,\delta_1^m$. For perspective, consider that the maximum displacement thickness δ_1^m is almost exactly one third of the viscous boundary layer thickness δ_v. This means that the presence of the plate edge is inducing a pressure spike at 90 viscous thicknesses above the plate even seven meters from the front plate edge. The pressure

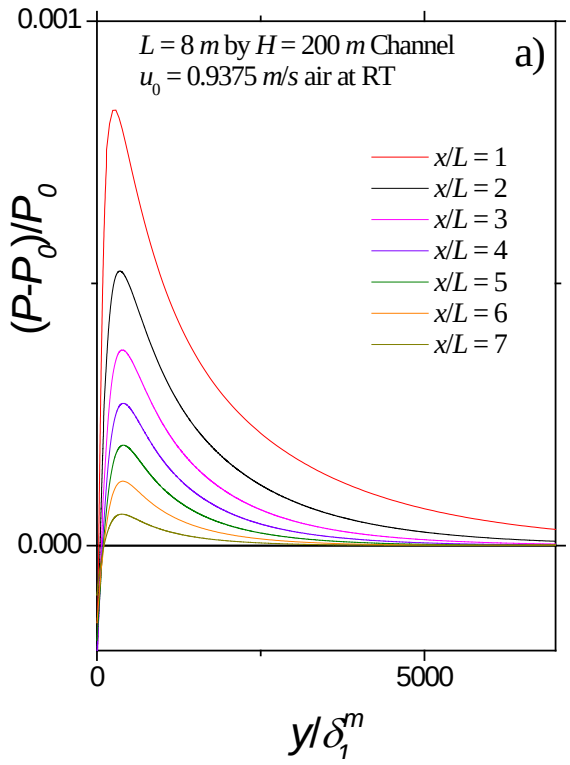

Figure 9a: The pressure profiles at different channel positions.

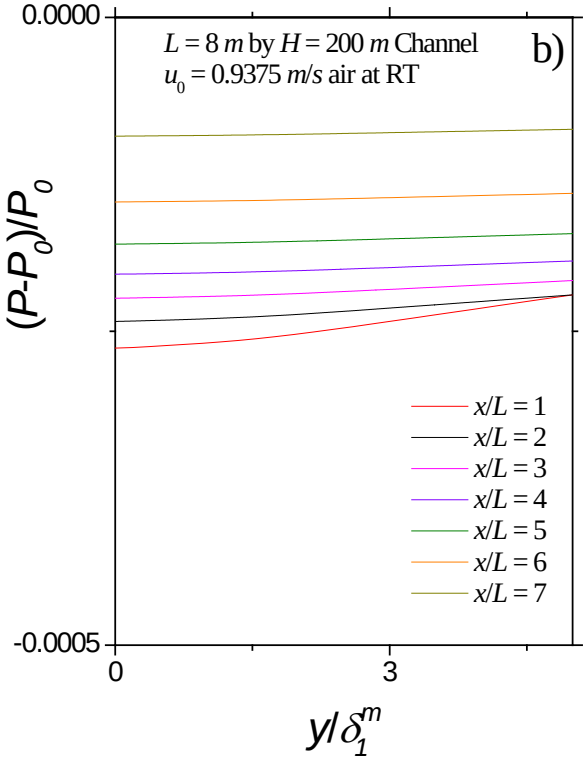

Figure 9b: Same as Figure 9a but only showing the near wall region.

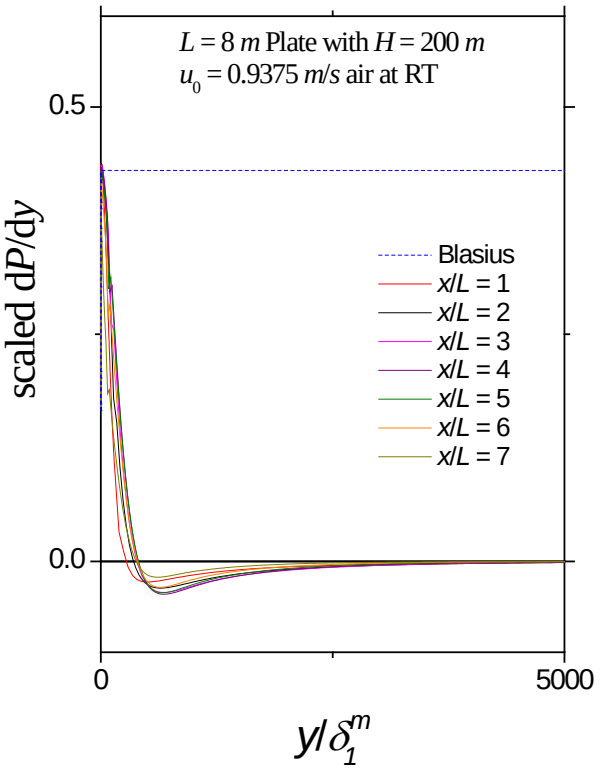

Figure 10a: The *y*-pressure gradient profiles at different channel positions.

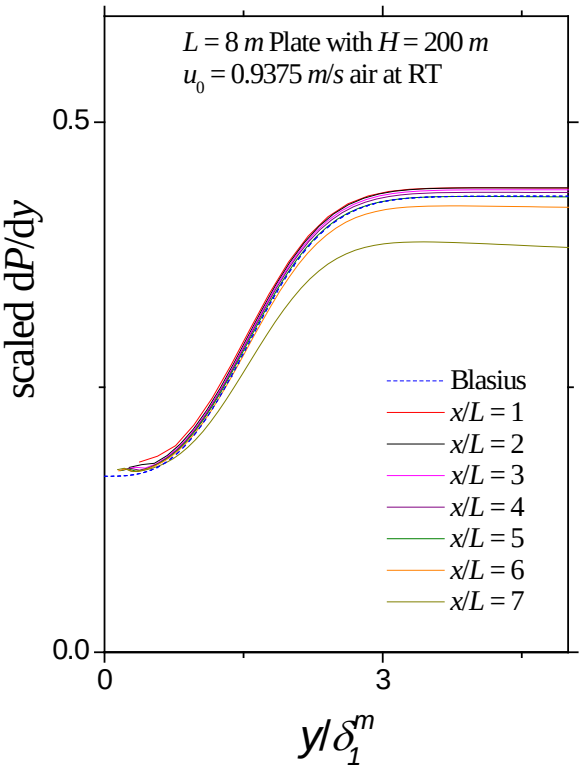

Figure 10b: Same as Figure 10a but only showing the near wall region.

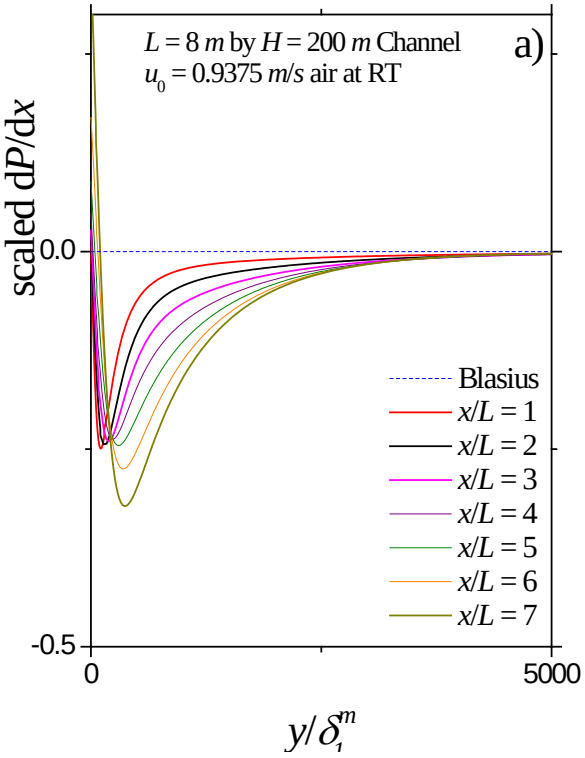

Figure 11a: The *x*-pressure gradient profiles at different channel locations.

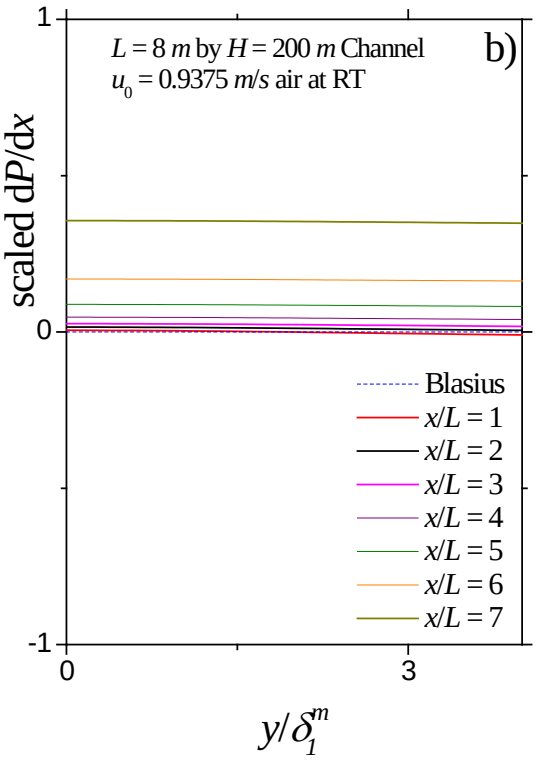

Figure 11b: Same as Figure 11a but only showing the near wall region.

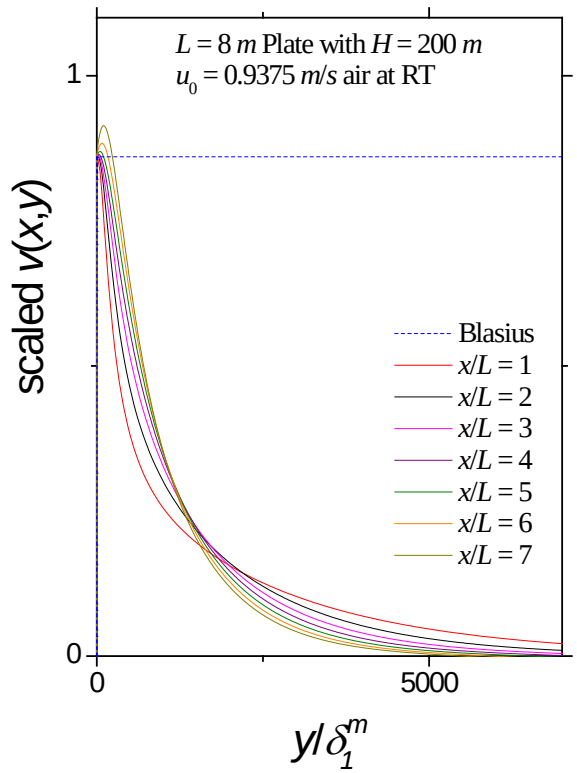

Figure 12a: The half channel *v*(x,y) velocity profiles at different channel positions.

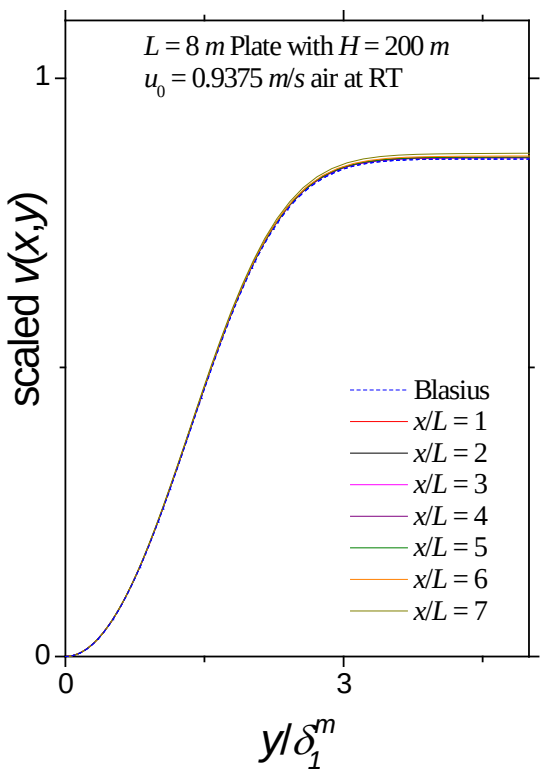

Figure 12b: Same as Figure 12a but only showing the near wall region.

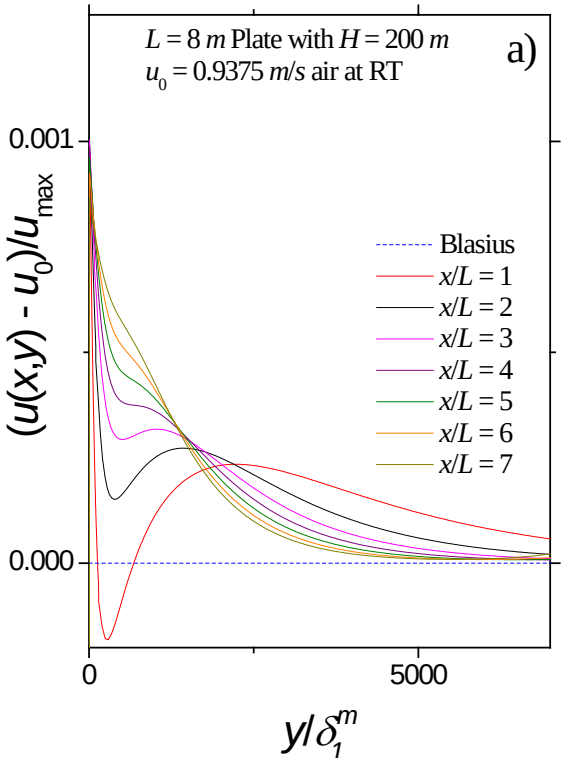

Figure 13a: The half channel *u*(x,y) velocity profiles at various channel

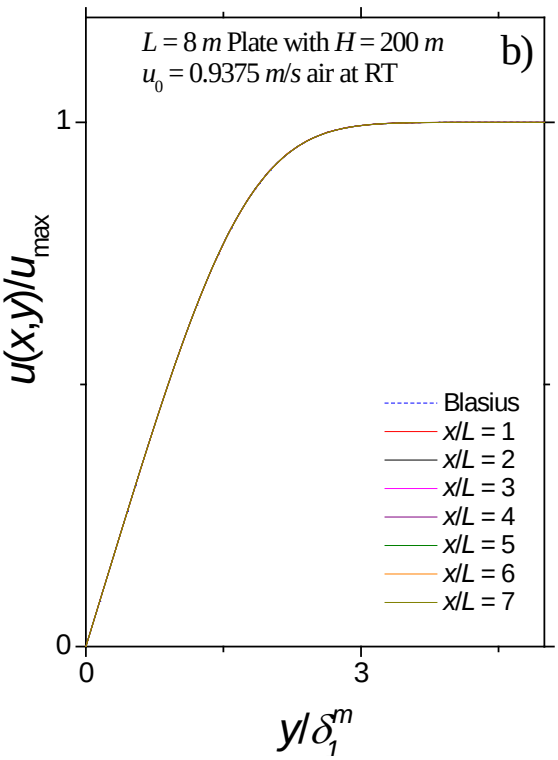

Figure 13b: Same as Figure 13a but only showing the near wall region.

effects extend thousands of viscous thicknesses above the plate. These type of very large length scales relative to the viscous boundary layer thickness emphasize the fact that it is the pressure disturbance at the plate edge that is playing a large role in the behavior of the fluid flow along the plate. Note that in the traditional Blasius boundary layer concept, the pressure effects due to the plate edge are ignored and assumed to be the same as the pressure in the free stream. The traditional assumption is that the pressure at each location along the plate would show no peak behavior; they would all be flat constant lines consistent with the Bernoulli-Euler equation. For the near wall regions (Fig. 9b), the most notable feature is that all the locations show negative pressures relative to the outlet pressure.

In Figs. 10 and 11 the associated *y* and *x* pressure gradient profiles are plotted at the same seven locations along the channel. The *y*-pressure gradients all behave in a similar fashion: they peak near the viscous-inertial boundary and then slowly decay to zero. The near wall region plots of d*P*/d*y* (Fig. 10b) show similar behavior except for the *x*/*L*=7 position closest to the exit. The d*P*/d*x* profiles in Fig. 11a clearly show the effect of the changing pressure difference peaks (Fig. 9a) in the inertial boundary layer region. The near-wall d*P*/d*x* cases in Fig. 11b are relatively constant but do not show similar behavior. Note that we used the same pressure gradient scaling for both the *x* and *y* cases to show that the pressure gradient effects are of the same order of magnitude. According to Blasius theory, the d*P*/d*x* profiles should scale as $u_{\max}^2 / x$ but plots (not shown) using this scaling also do not show similar behavior.

The $u(x, y)$ and $v(x, y)$ velocity profiles are plotted in Figs. 12 and 13. The near wall regions (Figs. 12b and 13b) both show similar-like behavior. If we plot just the scaled $u(x, y)$ profiles, they would all look identical since the u_{max} values are all similar in value and only about 0.1% larger than u_0. However, this 0.1% change is important in the inertial region since it is the same order of magnitude as the normal velocity $v(x, y)$. To emphasize this, in Fig. 13a, we plot $u(x, y) - u_0$ profiles rather than $u(x, y)$ profiles. This plot clearly shows the influence of the pressure peaks (Fig. 9a). On the other hand, the $v(x, y)$ velocity profiles (Fig. 12a) show something close to similar-like behavior in the inertial region and do not appear to be affected by the pressure peak change. Based on the Prandtl momentum equations, we expect and actually observe that the behavior of the dP/dy and the $v(x, y)$ velocity profiles are correlated as are the dP/dx and the $u(x, y)$ velocity profiles.

4. LAMINAR BOUNDARY LAYER THEORETICAL MODEL

The above simulation results provide us with the insight we need to develop a complete theory for unbounded laminar boundary layer flow. The key to the new theoretical model is the recognition that for unbounded flow on a flat plate, the flow must behave as depicted in Fig. 2. For theoretical convenience, we divide the unbounded boundary layer into two regions: the first is the viscous region which closely mimics the traditional viscous boundary layer, and the second region we termed the inertial region since viscous forces are mostly absent.

4.1 Near Wall Region

As in the traditional model, we assume a no-slip boundary condition at the wall which means that the velocity at the wall is zero. The velocity $u(x, y)$ monotonically increases from zero to a peak velocity we denote as $u_{\max}(x)$ (in the traditional model, the equivalent velocity is $u_e(x)$, the velocity at the viscous boundary layer edge). Herein, we choose to work with $u_{\max}(x)$ but as we noted earlier,[13,16] one could instead use the viscous boundary layer thickness $\delta_v(x)$. The peak velocity is induced by the localized pressure disturbance along the wall in the flow direction that is generated when the main flow encounters the slow-moving boundary layer flow. The pressure disturbances induced by the plate edge combined with the slow moving boundary layer flow not only results in the peak velocity in $u(x, y)$, but is also responsible for inducing the $v(x, y)$ velocity field. The near-wall viscous boundary layer thickness $\delta_{\max}(x)$ is considered to be the point where the velocity reaches the peak velocity $u_{\max}(x)$. The near wall boundary layer quantities like the displacement thickness and momentum thickness are all calculated relative to this peak velocity and thickness location.

The velocities and pressure gradients in this region are obtained using the standard Blasius[2] similarity approach using η and $f(\eta)$ but with the upper extent set to $\delta_{\max}(x)$ instead of infinity. The relevant equations are detailed in Appendix A. Besides the upper extent change, the big difference between the present formulation and the traditional formulation is the identification of the similarity scaling parameters. Weyburne[18] previously proved for 2-D fluid flow behaving as shown in Fig. 1, that if similarity is present in a set of velocity profiles then the velocity similarity scaling parameter must be $u_e(x)$ and the length scaling parameter must be the traditional displacement thickness $\delta_1(x)$. In Appendix B we offer a similar proof that the similarity scaling parameters for the new unbounded Blasius model are $u_{\max}(x)$ as the velocity scaling parameter and the length scaling parameter as the maximum displacement thickness $\delta_1^m(x)$ given by

$$\delta_1^m(x) = \int_0^{\delta_{\max}} dy \left\{ \frac{u_{\max} - u(x, y)}{u_{\max}} \right\} . \quad (1)$$

The experimental simulation results show in Figs. 10b, 12b and 13b confirm that the new scaling parameters result in similar-like behavior for the velocity and pressure gradients in the near wall region. The exception is the *x*-pressure gradient (Fig. 11b). Blasius theory assumes the *x*-pressure gradients should all be zero. What we have verified using the Bernoulli-Euler pressure gradient equation is that all of the profiles in Fig. 11b correspond to very small angle wedge flows, *i.e*. the *x*-pressure gradient is almost zero.

4.2 Inertial Region

With the near wall theoretical model in hand, we now turn to the inertial region. The inertial boundary layer region above the viscous region is characterized by a boundary layer thickness $\delta_i(x)$ and a very slow decay to the free stream velocity u_0. The viscous forces are mostly absent in this region. In earlier AF Tech Reports,[13,16] we speculated that similar-like solutions to the velocities in this region might be possible for the flat plate case. However, examination of Figs. 10-13 reveals that strictly similar solutions do not look possible using the near wall scaling parameters or any other scaling parameters. The $u(x,y)-u_0$ profile figures (Fig. 13a), in particular, do not look like any set of scaling parameters could make the profile plots look similar. While the near wall scaling parameters do not meet the strict standards for similarity, it does appear to scale the simulation profiles (for example Figs. 10 and 12) amplitudes and widths to the point that a simple analytical curve should work for most of the *x*-values along the plate. Since strict similar solutions are not possible, we will pursue an approximate approach using the near wall scaling parameters in combination with the near wall asymptotes as the lower boundary conditions.

4.2.1 The Inertial Velocity Approximation

Using the experimental evidence as a guide (Fig. 13), we assume that the $u(x,y)$ in the inertial region can be approximated by an exponential term that has the $u_{\max}$ value at the inertial boundary layer edge (at $y=\delta_{\max}$) and then slowly decreases into the free stream u_0. A reasonable approximation for the $u(x,y)$ velocity in the inertial region is

$$u_{exp}(x,y) \;=\; u_0+(u_{\max}-u_0)e^{-c(y-\delta_{\max})/\delta_1^m} \qquad for \qquad y\ge\delta_{\max} \quad , \tag{2}$$

where *c* is a constant. The *c* constant is found using the analytical $v(x,y)$ formula found by substituting Eq. 2 into the Prandtl mass conservation equation. By integrating the resulting conservation of mass equation, it is straightforward to obtain the analytical expression for the normal velocity $v(x,y)$ as

$$v_{exp}(x,y) \;=\; \frac{(u_{exp}\text{-}u_0)(cxy+x\delta_1^m)}{2cx^2}-\frac{(u_{\max}-u_0)\delta_1^m e^{c\delta_{\max}/\delta_1^m}}{2cx}-0.8604\sqrt{\frac{\nu u_{\max}}{x}} \quad for \quad y\ge\delta_{\max}. \tag{3}$$

The normal velocity $v_{exp}(x, y)$ will be near zero at the inertial boundary layer edge when $c \cong (u_{\max} - u_0)/u_{\max}$. The value of $\delta_1^m(x)$ is well approximated by the Blasius formula for the displacement thickness but with $u_{\max}$ replacing u_0 (see Appendix C). For $\delta_{\max}(x)$ we use the formula from the earlier paper[13] which works out to $\delta_{\max}(x) \cong 4.6\,\delta_1^m(x)$.

The only unknown at this point is the value of $u_{\max}(x)$. Although we believe an approximate expression is possible, the fact that $u_{\max}(x)$ is essentially a constant for a given u_0 and kinematic viscosity means that the development of the approximation would require a much bigger simulation effort. Herein, we will be satisfied in just laying out the general aspects of the analytical expression for the velocities in the inertial boundary layer region. To that end, we will use the measured $u_{\max}(x)$ values instead of an approximate expression.

With that set, we are now able to generate approximate velocity profiles for the conditions for air flow with $u_0 = 0.9375$ *m/s* and $\nu = 1.5E-5$ m^2/s. In Fig. 14 and 15 we plot $u(x, y)$ and $v(x, y)$ profiles for the simulation results and the approximate result at three positions along the plate. The comparison between the Blasius result and the near wall simulation result is excellent in both cases. The inertial results are not nearly as good but they do seem to have the right asymptotic behavior. Overall, this is about as good as can be expected considering the complex behavior of the simulation results in the inertial boundary layer region.

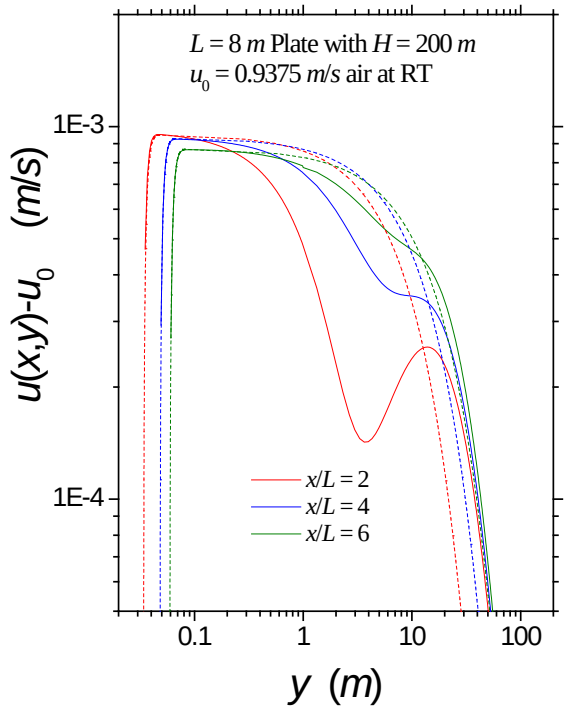

Figure 14: The half channel $u(x,y)$-u_0 velocity profiles at three channel positions. The solid lines are simulation and the dashed are the approximate results.

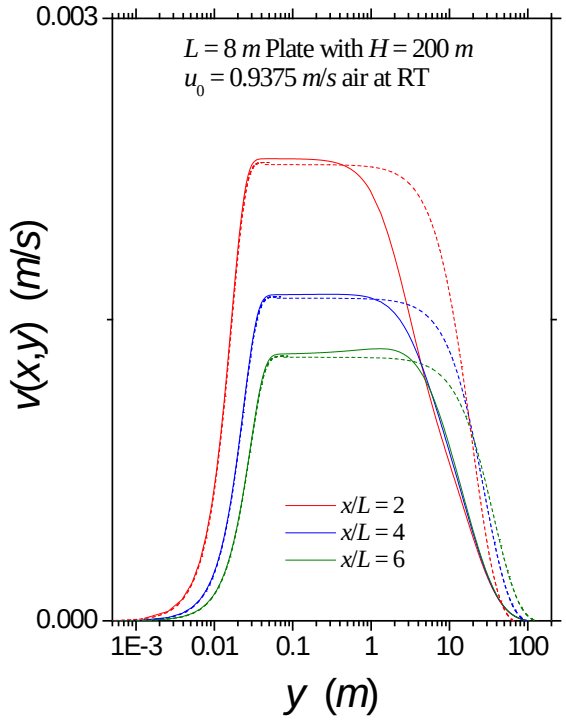

Figure 15: The half channel $v(x,y)$ velocity profiles at three channel positions. The solid lines are simulation and the dashed are the approximate results.

5. DISCUSSION

The main intent of this research has been to develop a realistic theoretical model for laminar flow over a flat plate. For the past one hundred years, it has been assumed that the Blasius flow model as depicted in Fig. 1 with u_0 replacing $u_e(x)$ is this model. And in fact, the flow depicted by Fig. 1 coupled with the Blasius theory is actually not too bad an approximation for the external flow case. For an external flow, we expect that the $u(x, y)$ velocity profiles should show a maximum but for the above unbounded flow case, the velocity maximum, u_{max}, is only 0.1% of u_0 for the conditions we used. In a wind tunnel, this difference would not be resolvable. While not a bad approximation, the problem is in the nonphysical or incorrect assumptions that come with the model. As we pointed out in the Introduction, the Blasius theoretical model as traditionally expounded falls short of what one would expect for laminar flow over a flat plate. In the traditional Blasius treatment, the boundary layer does not show any maximum. Furthermore, the finite nature of the calculated $v(x, y)$ velocity[9-11] and the *y*-pressure gradient[12] at infinite distance above the plate is not easily rationalized in the traditional approach. The misleading assumptions about the *x*-pressure gradient and the *y*-pressure gradient result in a false picture of the pressure field above the plate. Due to the close association between the Blasius model and the depiction of boundary layer flow, many of these incorrect assumptions from the Blasius theoretical model development have been incorporated into the *de facto* model for laminar flow over a flat plate.

What our research has uncovered is that the problem is not so much the Blasius model, but the conceptual model for the boundary layer. The traditional boundary layer concept has evolved from Prandtl's initial conceptualization to that model which corresponds to the boundary layer that is routinely measured in the wind tunnel and depicted in Fig. 1. Therein lies the first problem. Wind tunnel flow corresponds to an interior flow, not an exterior flow. In a wind tunnel, the velocity asymptotes to the boundary layer edge velocity $u_e(x)$ which, in general, is different than the free stream velocity u_0. This type of asymptotic behavior is a characteristic of an interior flow. A second problem with the conceptual model specific to the Blasius theoretical model has to do with the assumption that the asymptotic velocity is u_0. For an interior flow along a flat plate channel/conduit, the velocity above the flat plates can **never** reach u_0 since the boundary layers along the walls effectively narrows the interior volume so that $u_e(x)$ will always be larger than u_0 for incompressible fluid flow. (For example, in the earlier simulation for the 1-meter gap channel,[13] we found that the $u(x, y)$ asymptotic velocity is 3% higher than u_0 at x/L=7/8 and that the tail region velocity is relatively constant with a std. dev. less than 0.1%). The flow only asymptotes to u_0 for an exterior flow. Thus, we are in a situation where the traditional depiction of boundary layers in Fig. 1 has characteristics of both an exterior flow (no upper bound) and an interior flow (asymptotes to $u_e(x)$). At the same time, the Blasius theoretical model which is closely associated with the Fig. 1 depiction, also has characteristics of both exterior flow (upper bound u_0) and interior flow (the velocity profile asymptotes like an interior flow).

The flow community has been accepting of this mixed up traditional model since Blasius type velocity profiles like those depicted in Fig. 1 are routinely measured in wind tunnels. However, as we pointed out in the Introduction, simulations of wind tunnel profiles only match the $u(x, y)$ Blasius profiles, but do not match the $v(x, y)$ profiles or the y-pressure gradient profiles. Therefore, the long-standing assumption that Blasius theoretical model can describe certain wind tunnel velocity and pressure fields like those depicted in Fig. 1 is not correct.

The bottom line is that the boundary layer concept that has been developed and presented to the flow community for laminar flow on a flat plate is **not** correct. The results herein indicate that there is a way forward. The path is twofold. First, we redefine the traditional depiction of boundary layer flow in terms of the bounded and unbounded boundary layer concepts. In Fig. 2 above, we depict the unbounded boundary layer concept. This is the type of boundary layers we expect in most exterior flows and some interior flows (*e.g.*, 200-meter gap 2D channels). As we demonstrated above, most of the theoretical problems and conceptual problems with the Blasius theoretical model all go away if it is applied to the unbounded boundary layer concept.

The second part of our boundary layer fix is to reimagine the bounded boundary layer case. This is done by replacing the traditional depiction shown in Fig. 1 with Fig. 16. The difference between the two figures is that we have added the $H/2$ dashed line to connotate that this is an interior flow situation and that there are undocumented pressure fields that produce the shown asymptotic velocity behavior.

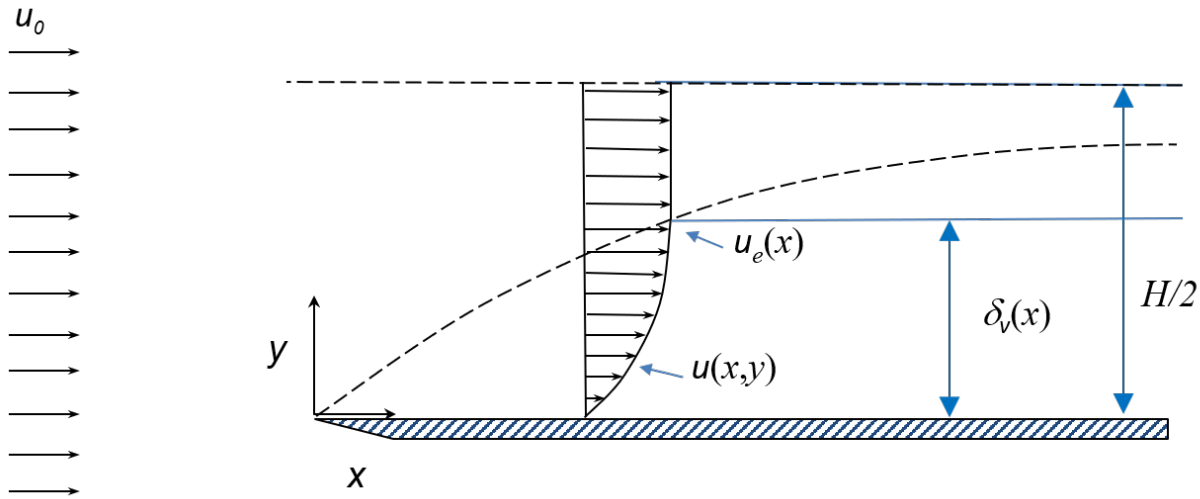

Figure 16: The revised depiction of the 2-D "bounded" boundary layer along a semi-infinite flat plate. Not to scale since, in general, $\delta(x) << H/2$.

It should be pointed out that it is possible to have boundary layers that fall in between these two types of representative boundary layer types (*e.g.*, the 75-meter gap case discussed above). For clarity, we note the possibility but only formalize the two main versions. There is no sharp division between the bounded and unbounded boundary layers. For example, one could define the border between the two by when the Blasius-like behavior in the near wall region starts (at

10-meter gap 2D channel[13]) or, alternatively, when the velocities and pressure gradients all show slow asymptotic behavior to zero (as above for the 200-meter gap channel).

For the flat plate case, the difference in the $u(x, y)$ velocity profiles between the bounded and unbounded flow cases is small. The velocity maximum, u_{max}, is only 0.1% of u_0 for the conditions we used. Where the differences will become very noticeable is once we start examining the titled plate case. For example, for the airflow over a NACA 0012 wing section we examined in an earlier report,[13] we found u_{max} values 15% higher than u_0. For the tilted plate case in which a favorable pressure gradient develops, the new boundary layer concept can be depicted by slightly modifying Figs. 2 and 16. The flow will still show a maximum for the velocity profile. However, for a tilted plate resulting in an adverse pressure gradient, there is no flow maximum but a flow deficit instead. For this case, it will be necessary to replace δ_{max} by δ_v and u_{max} by $u_v = u(x,\delta_v)$. As we noted previously,[13] for the flat plate case, either set of parameters will work as the dividing point between the viscous boundary layer and the inertial boundary layer regions since their values are close.

The second objective of the work herein is to flesh out the physics that goes with the new conceptual models for boundary layer flow. Perhaps the biggest difference between the bounded and unbounded boundary layer concepts is presence of the velocity maximum in the $u(x, y)$ velocity profile. Our assertion is that this maximum is a result of the same pressure field that is generating the normal $v(x, y)$ velocities. And, in fact, we showed in Figs. 10 and 11 that the x and y pressure gradients are of the same order of magnitude in roughly the same spatial location. This fact is reinforced by looking at the relative velocity fields. In Fig. 17 we replot the simulated normal velocity profiles from Fig. 12 but scale the $v(x, y)$ velocities by the excess $u(x, y)$ velocity given by $u_{max} - u_0$. What we see is that the normal velocity $v(x, y)$ is within a factor of 2-3 times the excess $u(x, y)$ velocity. Hence, the boundary layer pressure fields that are

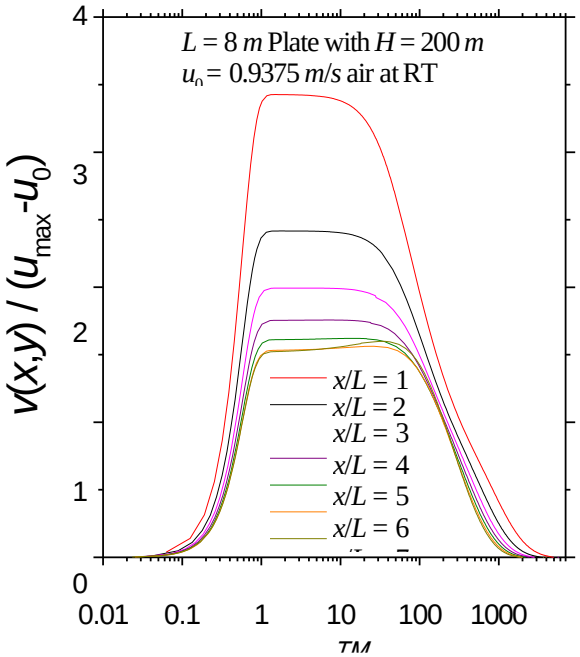

Figure 17: The half channel $v(x,y)$ velocity profiles at different channel positions but scaled by u_{max}-u_0.

generating the normal velocity are also generating a similar magnitude excess $u(x, y)$ velocity field. The velocity peak only manifests when the pressure field in the boundary layer region is not swamped out by the imposition of another pressure field (like for the case of the bounded boundary layer).

Perhaps the most damaging aspect of the traditional conceptual model is the acceptance of the Blasius model as representative of the actual pressure environment surrounding the plate. It is very common in the literature[12] to find claims that the *y*-pressure gradient is zero in the boundary layer region. Together with the Blasius assumption that the *x*-pressure gradient is zero, one could conclude that there are **no** pressure effects for boundary layer flow. Most literature treatments of the boundary layer offer no counter to these misleading aspects of the pressure fields surrounding the boundary layer. The result is that the total neglect of the pressure fields has been incorporated into the traditional conceptual model of the boundary layer. To counter this, we show the pressure distribution obtained for the 200 *m* gap channel flow at one of the channel edges in Fig. 17. The absolute pressure changes are relatively small at about 0.1%, but the effects are felt many tens of meters away. Examination of Figs. 9-11 give a snapshot of the pressure and pressure gradients above the plate at various locations along the plate.

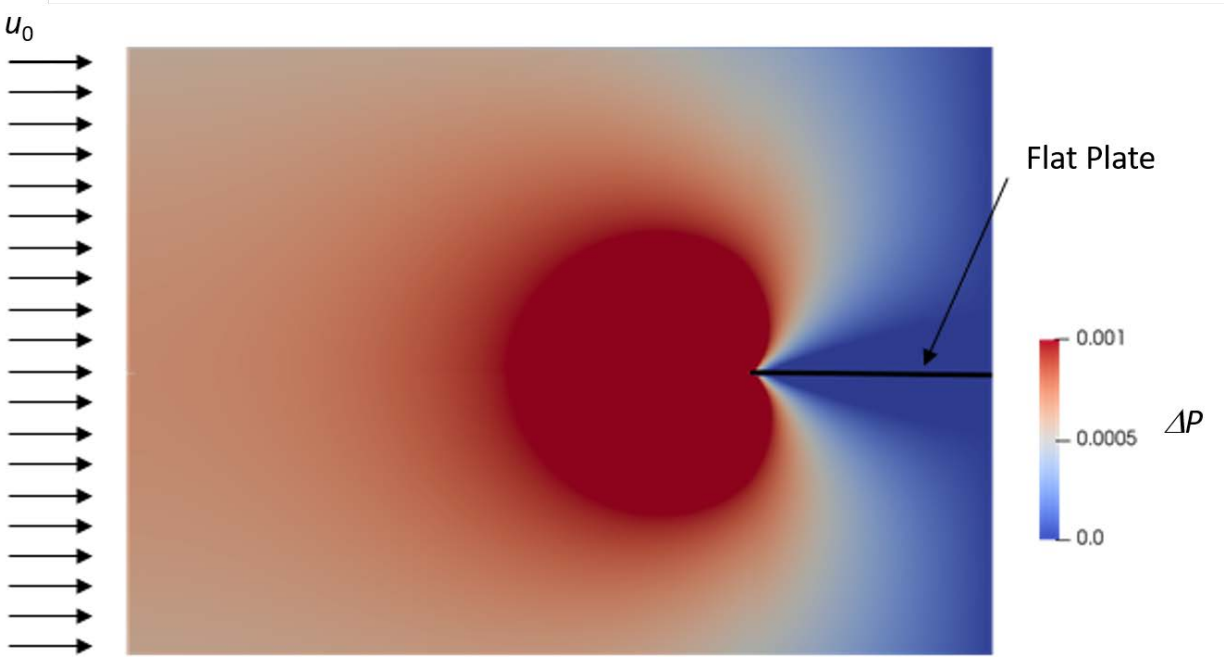

Figure 18: Simulated pressure field around a flat plate for airflow at u_0=0.9375 *m*/*s*.

For comparison, we plot a snapshot of the pressure field for a bounded 1-meter high gap channel representative of a typical wind tunnel in Fig. 19. The pressure field is very different. First, the pressure inside the channel is at least an order of magnitude larger than in the unbounded case. The *x*-pressure gradient along the channel center line is 10,000 times larger in the 1-meter gap versus the 200-meter gap channel. Secondly, the pressure along the normal direction at any location along the plate (not shown) for the bounded flow case is nearly constant, even in the viscous boundary layer region. In contrast, the pressure and the *y*-pressure gradient are not constant (Figs. 9 and 10) for the unbounded flow case. Thus, the pressure fields for the two

cases are very different even though the scaled $u(x, y)$ velocity profiles along the plates look almost identical.

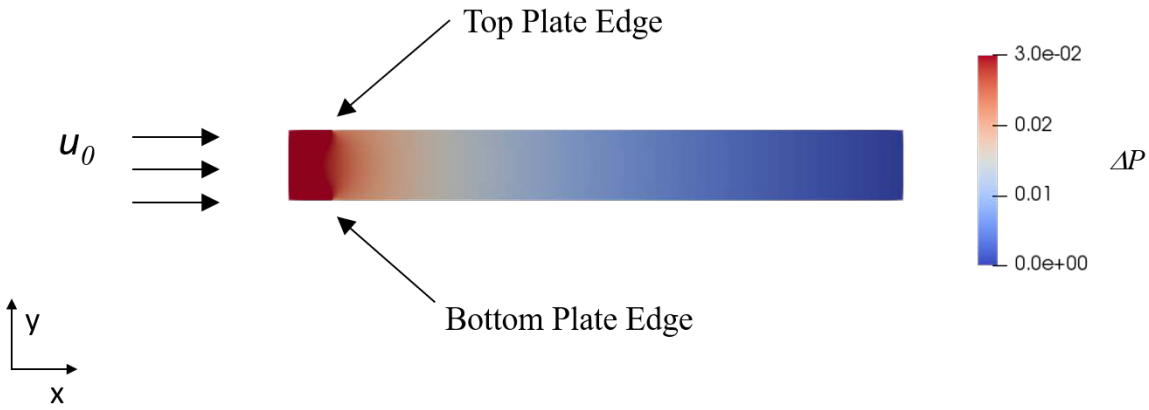

Figure 19: Simulated pressure field around a 2D flat plate channel with typical wind tunnel dimensions (1-meter by 8-meter) with inlet airflow at u_0=0.9375 m/s.

The big difference in wind tunnel and exterior pressure fields has implications that need careful review. It has always been the contention of experimentalist that the results obtained in the wind tunnel are equivalent to the exterior flow case. That is, simulating flow over a wing in a wind tunnel is equivalent to flow over a wing in free flight. It is clear that the flow along the wing dominates the overall flow in terms of magnitude and energy content and, in this way, the flows are similar. However, the processes that involve stability and transitions involve small perturbations to the flow. It is not unreasonable to expect that those perturbations could be affected by the pressure field and normal velocity field in which case the point where/when a transition takes place could be different for the two cases. One way to try to address this is through computational fluid flow studies.

A related issue to this wind tunnel and exterior flow issue concerns the common practice of setting up wind tunnel experiments to have Blasius velocity profiles. Since experimentalists could not, and still cannot, measure the velocities and pressures with sufficient accuracy and spatial precision, they often attempt to put the plate in the wind tunnel into a flow state where all of the pressure gradients and velocities are known. Hence, the common practice of setting up wind tunnel conditions that produce Blasius profiles along the plate. However, as we discussed above, computer simulation results[13] indicate that this supposedly known state condition is illusionary, only the $u(x,y)$ profiles show similarity, the normal velocity and the pressure gradient profiles do not show similarity. This means the normal velocities and the normal pressure gradients are not known. For certain experiments involving stability or laminar-turbulent transition, one can speculate that small disturbances would respond differently depending on the normal velocity and the y-pressure gradient condition on the plate. Hence, stability would be affected. This also may be something simulation studies could elucidate.

What is also clear from our simulation results to date is that large gap 2D channel flow is not like parabolic velocity flow encountered in plane Hagen-Poiseuille (channel) flow treated in many textbooks. The Hagen-Poiseuille flow assumes viscosity is active throughout the channel. This

will only occur when the channel gap is on the order of the viscous boundary layer thickness. For the airflow used herein, that would correspond to a gap of about 0.04-meters. Once the channel gap reaches about 3-4 viscous thicknesses, the velocity profile changes from parabolic to a flat top curve (Fig. 16). This type of curve persists until the channel gap reaches about 1800 viscous thicknesses at which point the flow starts to show a velocity profile maximum. Once the channel gap reaches about 5000 viscous thicknesses, the flow is completely unbounded and behaves like an exterior flow.

The bounded and unbounded boundary layer descriptions have been limited to the laminar flow case. We need to modify the description for the turbulent boundary layer case. This should be relatively straightforward for the bounded boundary layer case. The bounded turbulent boundary layer shows the same type of asymptotic behavior as for the laminar case, i.e. it slowly asymptotes to the edge velocity $u_e(x)$ in the near wall region. For the unbounded boundary layer case, it is not obvious how this would play out. Although there are plenty of turbulent boundary layer datasets available, it is not certain that any of these represent truly unbounded turbulent boundary layers. Since all wind tunnel experiments appear to be bounded, the computer simulation path is the only path available for generating unbounded turbulent boundary layers. It is not clear whether the simulations involving RANS turbulence models (such as Spalart-Allmaras) would work since it is not known whether the turbulence models correctly approximate unbounded flows. That leaves DNS simulation as the only viable option. Given the very large domain size that would be required (at least 5000 viscous thicknesses from each boundary), the DNS calculation becomes very time consuming.

6. CONCLUSION

A new theoretical model for laminar flow over a flat plate is developed. The key to the development is not the theoretical model but the new unbounded boundary layer conceptual model. The new theoretical model is divided into two regions, the near wall region and the inertial region. In the near wall region, we reapply the Blasius theoretical model in a context that removes the theoretical problems. With the aid of a computer simulation study, a simple approximate analytical model is introduced for the inertial region. The resulting model is found to compare reasonably well with simulation results. The results are used to put the bounded and unbounded conceptual models into better focus.

ACKNOWLEDGMENT

The author acknowledges the support of the Air Force Research Laboratory and Gernot Pomrenke at AFOSR.

7. REFERENCES

[1]L. Prandtl, "Über Flüssigkeitsbewegung bei sehr kleiner Reibung," Verhandlungen des Dritten Internationalen Mathematiker-Kongresses in Heidelberg 1904.

[2]H. Blasius, "Grenzschichten in Flüssigkeiten mit kleiner Reibung," Zeitschrift für Mathematik und Physik, **56**, 1(1908).

[3]J. Nikuradse, Laminare Reibungsschichten an der längsangetrömten Platte. Monograph, Zentrale f. wiss. Berichtswesen, Berlin, 1942.

[4]H. Schlichting, *Boundary-Layer Theory*, 7*th* ed., McGraw-Hill, New York ,1979.

[5]J. Jovanović, B. Frohnapfel, E. Škaljić, and M. Jovanović, "Persistence of the Laminar Regime in a Flat Plate Boundary Layer at very High Reynolds Number," Thermal Science, **10**, 63(2006).

[6]N. Patten, T. M. Young, and P. Griffin, "Design and Characteristics of New Test Facility for Flat Plate Boundary Layer Research," Proc. World Acad. Sci., Eng. and Tech., **58**, 366(2008).

[7]J. Slater, J. Dudek, and K. Tatum, "The NPARC Alliance Verification and Validation Archive", NASA/TM-2000-209946, ASME 2000-FED-11233, 2000.

[8]U. Ghia, S. Bayyuk, S. Habchi, C. Roy, T. Shih, T. Conlisk, C. Hirsch, and J. Powers, "The AIAA code verification project - Testcases for CFD code validation," AIAA 2010-0125, 2010.

[9]J. Lewins, "Beyond the boundary layer: the Blasius paradox," Int. J. Mech. Engr. Educ., **27**, 55(1999).

[10]R. Panton, *Incompressible Flow*, 3rd ed., John Wiley, New Jersey, 2005.

[11]A. Pantokratoras, "Is the ambient transverse velocity in a boundary layer flow non-zero or zero?" arXiv:1002.1787 [physics.flu-dyn], 2010.

[12]D. Weyburne, "The Normal to the Wall Pressure Gradient for Blasius and Falkner-Skan Boundary Layer Flow," AF Tech Report AFRL-RY-WP-TR-2018-0153, https://discover.dtic.mil/, 2018.

[13]D. Weyburne, "The Unbounded and Bounded Boundary Layer Models for Flow Along a Wall," AF Tech Report AFRL-RY-WP-TR-2019-0002, https://discover.dtic.mil/, 2018.

[14]Z. Harun, J. Monty, R. Mathis, and I. Marusic, "Pressure gradient effects on the large-scale structure of turbulent boundary layers," J. Fluid Mech., **715**, J. Fluid Mech., 477(2013).

[15]J. Klewicki, W. Saric, I. Marusic, J. Eaton, "Wall-Bounded Flows", Chapter 12, in

C. Tropea, A. Yarin, and J. Foss, Springer Handbook of Experimental Fluid Mechanics, Springer-Verlag Heidelberg, 2007.
[16]D. Weyburne, “A Boundary Layer Model for Unbounded Flow Along a Wall,” AF Tech Report AFRL-RY-WP-TR-2019-0001, https://discover.dtic.mil/, 2019.

[17]M. Vaughn, “Guidelines for Gridding Simple Flows- The Flat Plate in Laminar Flow,” Army Tech. Report TR-AMR-SS-08-09, A476652, https://discover.dtic.mil/, 2009.

[18]D. Weyburne, “Similarity of the Velocity Profile,” AF Tech Report AFRL-RY-WP-TR-2014-0221, https://discover.dtic.mil/, 2014.

APPENDIX A: THE BOUDARY LAYER FORMULATION

In this Section, we outline our theoretical model for the boundless boundary layer. In the near wall region, we assume the flow behaves as a slightly modified Blasius model. The main differences are that the model only applies from the wall to $\delta_{\max}(x)$ and the scaling parameters become $u_{\max}(x)$ as the velocity scaling parameter and the length scaling parameter as the maximum displacement thickness $\delta_1^m(x)$ given by

$$\delta_1^m(x) = \int_0^{\delta_{\max}} dy \left\{ \frac{u_{\max} - u(x,y)}{u_{\max}} \right\} \quad . \tag{A1}$$

Weyburne[20] proved that if similarity is present in a set of velocity profiles that behave according to the traditional bounded boundary layer description depicted in Fig. 1, then the similarity scaling parameters must be $u_e(x)$ as the velocity scaling parameter and the length scaling parameter must be the traditional displacement thickness $\delta_1(x)$. In Appendix B we apply the same integral based method for the unbounded boundary layer for the near wall region from the wall out to $\delta_{\max}(x)$. It is found that if similarity exits in a set of velocity profiles, $\delta_1^m(x)$ and $u_{\max}(x)$ must be the similarity scaling parameters. This result applies for any 2-D flow that behaves as the unbounded flow depicted in Fig. 2.

Having identified the similarity scaling parameters as $\delta_1^m(x)$ and $u_{\max}(x)$, it is a simple matter to obtain solutions to the flow governing equations to the near wall region by following the approach of Blasius.[2] We assume $u_{\max}(x)$ is constant and that the maximum displacement thickness $\delta_1^m(x)$ is well represented by

$$\delta_1^m(x) = b\left(x - x_0\right)^n \quad , \tag{A2}$$

where x_0, b, and n are constants. These are testable propositions for experimental datasets that might display similar behavior and in Appendix C below we demonstrate that it works well for the *H*=200 *m* dataset developed above.

With the *x*-behavior of the scaling parameters in hand, the flow governing equations can be transformed into dimensionless form. The resulting momentum equations and their solution are identical to the standard Blasius equations but now applying only from the wall out to $\delta_{\max}(x)$ and $u_{\max}$ replacing u_0.

With the near wall region in hand, we now turn our attention to the inertial boundary layer region. In an earlier report, we speculated that it this region might have similar soluions.[13] However, examination of Figs. 10-13 reveals that, at least for the flat plate case, strictly similar solutions

do not look possible. While the near wall scaling does not meet the strict standards for similarity, it does appear to scale the simulation profiles (for example Figs. 12 and 13) amplitudes and widths to the point that a simple analytical curve should work for most of the *x*-values along the plate. Herein, our solution approach is to approximate the similar-like scaled $u(x,y)$ velocity profile. A reasonable approximation for the inertial velocity is

$$u_{exp}(x,y) \quad = \quad u_0 + (u_{\max} - u_0)e^{-c(y-\delta_{\max})/\delta_1^m} \qquad for \qquad y \geq \delta_{\max} \qquad , \tag{A3}$$

where *c* is a constant. The constant *c* is obtained by requiring normal velocity $v(x,y)$ to be zero in the free stream. By integrating the conservation of mass equation, it is straightforward to obtain the analytical expression for the normal velocity $v(x,y)$ as

$$v_{exp}(x,y) \quad = \quad \frac{(u_{exp}\text{-}u_0)(cxy + x\delta_1^m)}{2cx^2} - \frac{(u_{\max} - u_0)\delta_1^m e^{c\delta_{\max}/\delta_1^m}}{2cx} + k \quad for \quad y \geq \delta_{\max} \qquad , \tag{A4}$$

where *k* is the integration constant. The value of the integration constant is obtained by requiring the $v_{exp}(x,y)$ value at the viscous-inertial boundary to be the Blasius asymptotic value (0.8604) which means

$$k \quad \cong \quad 0.8604\sqrt{\frac{\nu u_{\max}}{x}} \quad . \tag{A5}$$

To make the normal velocity $v_{exp}(x,y)$ be zero in the free stream, then *c* must be

$$c \quad \cong \quad \frac{(u_{\max} - u_0)\delta_1^m}{2xk} \quad = \quad \frac{(u_{\max} - u_0)}{u_{\max}} \quad . \tag{A6}$$

The displacement thickness δ_1^m is calculated using the Blasius displacement thickness formula but with $u_{\max}$ replacing u_0 (see Appendix C). The only unknown at this point is the value of $u_{\max}(x)$. Although we believe an approximate expression is possible, the fact that $u_{\max}(x)$ is essentially a constant for a given u_0 and kinematic viscosity means that the development of the approximation would require a much bigger simulation effort. Herein, we will be satisfied in just laying out the general aspects of the analytical expression for the velocities in the inertial boundary layer region. To that end, we will use the measured $u_{\max}(x)$ values instead of an approximate expression.

The one other quantity needed above that is not commonly discussed[12] is the *y*-pressure gradient. The suitably scaled *y*-pressure gradient for the present situation is given by

$$-\frac{1}{u_{\max}^2 b(x-x_0)^{n-2}}\frac{1}{\rho}\frac{\partial p}{\partial y} \quad = \quad -\frac{(x-x_0)^{3/2}}{u_{\max}^{3/2}\sqrt{\nu}}\frac{1}{\rho}\frac{\partial p}{\partial y} \quad . \tag{A7}$$

APPENDIX B: SIMILARITY OF THE UNBOUNDED BOUNDARY LAYER

In an earlier AF Tech Report, Weyburne[18] developed an integral area approach to determine the similarity scaling parameters for the velocity profile for 2-D wall-bound boundary layer flows where the velocity profiles asymptote to $u_e(x)$. The approach is based on a simple concept; the area under a set of scaled velocity profile curves that show similarity behavior must be equal. This led to a new integral-based derivation that proved that if similarity is present in a set of velocity profiles, then the similarity scaling velocity parameter must be $u_e(x)$ and the similarity length scaling parameter must be the traditional displacement thickness $\delta_1(x)$. This proof works for the **bounded** boundary layer case where the flow asymptotes to $u_e(x)$ as shown in Fig. 16. In what follows, we present the equivalent similarity derivation for the near wall region of the **unbounded** boundary layer depicted in Fig. 2.

The derivation starts with the definition of velocity profile similarity. Assume that the length scaling parameter $\delta_s(x)$ and velocity scaling variable $u_s(x)$ result in a set of similar velocity profiles in the near wall region. Using the Schlichting[4] definition, the scaled velocity profile at a station x_1 along the wall is similar to the scaled profile at x_2 if

$$\frac{u\left(x_1, y/\delta_s\left(x_1\right)\right)}{u_s\left(x_1\right)} = \frac{u\left(x_2, y/\delta_s\left(x_2\right)\right)}{u_s\left(x_2\right)} \quad for \;\; y \le \delta_{\max} \qquad . \tag{B1}$$

The velocity $u(x,y)$ is written in this way to specify that the scaled velocity comparisons are made at the equivalent $y/\delta_s\left(x\right)$ values and **not** at the equivalent y-values. Similarity necessarily requires that if the scaled profiles are similar, then the scaled derivatives of the velocity profiles must also be similar. This, in turn, means that the derivative profiles plotted versus the similarity scaled y-value must have equal areas. In mathematical terms, the area under the scaled first derivative profile curve is expressed by

$$a\left(x\right) = \int_0^{\delta_{\max}/\delta_s} d\left\{\frac{y}{\delta_s}\right\} \frac{d\left\{u\left(x, y/\delta_s\right)/u_s\right\}}{d\left\{\dfrac{y}{\delta_s}\right\}} \qquad , \tag{B2}$$

where $a(x)$ is, in general, a non-zero value. For clarity, $\delta_{\max}(x)$, $u_s(x)$, and $\delta_s(x)$ have been shortened to $\delta_{\max}$, u_s, and δ_s. Using the appropriate boundary conditions $u\left(x,0\right)=0$, $u\left(x,\delta_{\max}\right)=u_{\max}\left(x\right)$, and a simple variable switch $\left(d\left\{y/\delta_s\right\} \Rightarrow \left(1/\delta_s\right)dy\right)$, Eq. B2 can be shown to reduce to

(B3)

$$a(x) \;=\; \frac{u_{\max}(x)}{u_s(x)} \quad .$$

Similarity requires that $a(x_1) = a(x_2)$. This result necessarily requires that if similarity is present in a set of velocity profiles in the near wall region, then $u_{\max}(x)$ must be a similarity velocity scaling parameter.

Next, consider the area under the velocity profile curves. Starting with the formal definition of similarity given by Eq. B1 then it is self-evident that for the profiles to be similar, the area under these scaled velocity profiles plotted versus the scaled *y*-coordinate must be equal. The area under the scaled profiles, in mathematical terms, is given by

$$b(x) \;=\; \int_0^{\delta_{\max}/\delta_s} d\left\{\frac{y}{\delta_s}\right\} \frac{u_{\max} - u(x, y/\delta_s)}{u_s} \quad , \tag{B4}$$

where $b(x)$ is in general a nonzero constant and where we have used the result from Eq. B3 to write the velocity in terms of the so-called defect profile. It is easily verified that similarity requires that $b(x_1) = b(x_2)$. Using a simple variable switch, Eq. B4 can be shown to reduce to

$$b(x) \;=\; \frac{\delta_1^m(x)\, u_{\max}(x)}{\delta_s(x)\, u_s(x)} \quad , \tag{B5}$$

where the δ_1^m is the maximum displacement thickness given by Eq. A1. (The reduction of the equivalent Eq. B2 and B4 integrals were outlined in detail in the earlier AF Tech Report[18]). Since similarity requires that $b(x_1) = b(x_2)$, then, combining with the Eq. B3 result, this result necessarily means that if similarity is present in a set of velocity profiles in the near wall region, then $\delta_1^m(x)$ must be a similarity length scaling parameter. This result applies to the near wall region of any unbounded 2-D fluid flow along a flat plate. The result is mathematically rigorous; it is only dependent on the definition of similarity, the definition of the displacement thickness, and the boundary conditions.

APPENDIX C: THE BOUDARY LAYER CHECK

The similarity theoretical development for the inertial boundary layer (Appendix A) made assumptions about the *x*-behavior of the scaling parameters $\delta_1^m(x)$ and $u_{\max}(x)$. These are testable assumptions for datasets that are believed to show similarity. The datasets above in

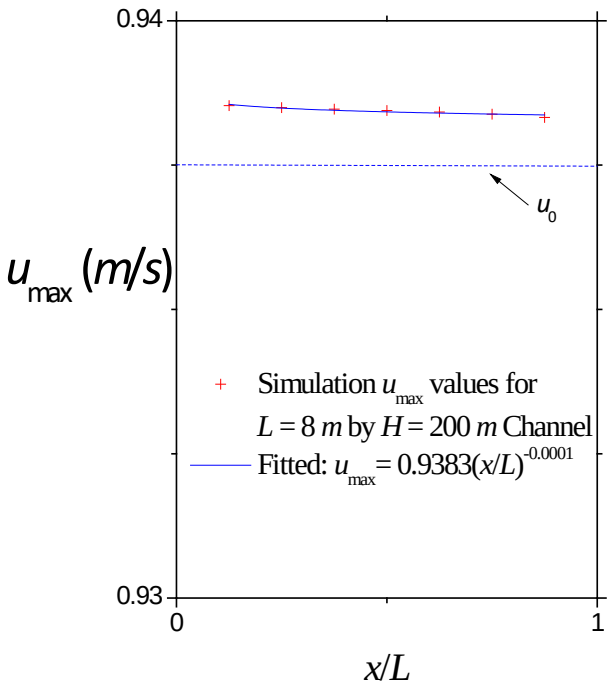

Figure C1: The maximum velocity at different stations along the channel with u_0 = 0.9375 *m/s*.

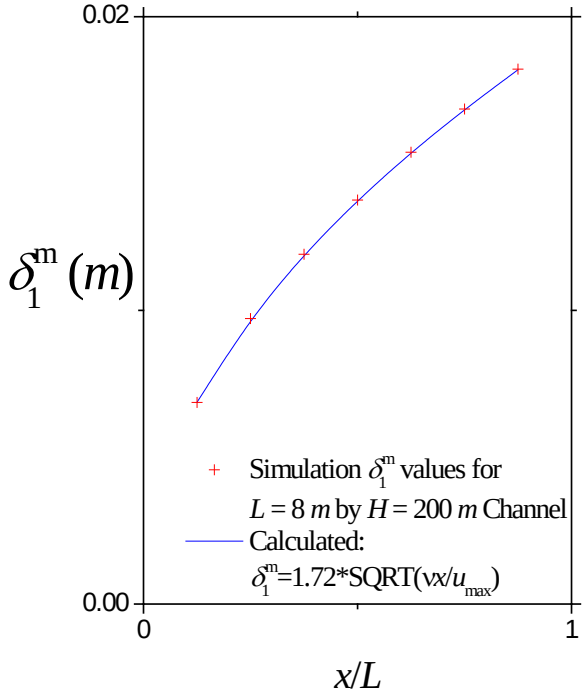

Figure C2: The inertial displacement thickness at different stations along the channel.

Section 3 are just such cases. For the profiles to show similar behavior, we need $u_{\max}(x)$ to be constant. Consider Fig. C1 in which we plot the $u_{\max}(x)$ for the simulation case L=8 *m* by H=200 *m* from Section 3. It is apparent that $u_{\max}(x)$ is indeed almost constant. The similarity assumption also requires that the scaling parameter $\delta_1^m(x)$ be well represented by simple power function of *x*. For the L=8 *m* by H = 200 *m* channel case, we found that the displacement thickness $\delta_1^m(x)$ is indeed well approximated using the standard Blasius values (Eq. A2) given by $n = 1/2$, $x_0 = 0$, and $b = 1.72\sqrt{\nu / u_{\max}}$ as is evident in Fig. C2. The calculated formula is the standard Blasius formula with $u_{\max}(x)$ replacing u_0.